AUTOMATED TRAVEL-TIME PICKING USING SPECTRAL RECOMPOSITION

Nelson Ricardo Coelho Flores Zuniga [iD][1,2*] and Viatcheslav Ivanovich Priimenko [iD][3]

ABSTRACT. To perform the velocity analysis by an inversion procedure, in which the calculated travel-times are compared to the observed ones, there is the necessity of obtaining the travel-time curve observed in the seismogram. However, obtaining the travel-time curve from a reflection event implies in a not-automated picking. Thus, in this work, we propose an automated travel-time picking technique, able to extract the travel-time curves from the target *PP* and *PSv* reflection events. Our proposed technique is based on recomposing the spectrum of frequencies of a wavelet by performing the inversion of the wave parameters, especially their amplitudes and peak frequencies. Then, the process is applied to each wavelet of a seismic trace, in which the comparison and cross-correlation among each spectrum, related to each wavelet, are performed. The process is, then, applied to each seismic trace, and, finally, the travel-time curve, related to the target reflection event, is determined. Our proposed technique shows to be effective when it is applied to reflection events from interfaces between the top of a pre-salt carbonate reservoir and the bottom of its salt structure.

Keywords: automated picking, inversion, spectral recomposition.

RESUMO. Para realizar a análise de velocidades segundo um procedimento de inversão, no qual os tempos de trânsito calculados são comparados aos observados, há a necessidade de obter-se a curva de tempos de trânsito observada no sismograma. Entretanto, obter a curva de tempos de trânsito de um evento de reflexão implica em fazer a seleção manual ou não automatizada destes tempos. Portanto, neste trabalho, uma técnica automatizada de seleção, capaz de extrair a curva de tempos de trânsito dos eventos *PP* e *PSv* alvo, é proposta. Essa técnica é baseada em reconstruir o espectro de frequências de uma ondaleta ao realizar a inversão dos parâmetros de onda, especialmente suas amplitudes e frequências dominantes. Então, o processo é aplicado para cada ondaleta de um traço sísmico, no qual a comparação e correlação cruzada entre cada espectro, relacionado a cada ondaleta, são realizadas. O processo é, então, aplicado a cada traço sísmico, e, finalmente, a curva de tempos de trânsito, relacionada ao evento de reflexão alvo, é determinada. A técnica proposta mostra efetividade, quando essa é aplicada em eventos de reflexão oriundos de interfaces entre o topo de um reservatório do pré-sal e o fundo de sua estrutura de sal.

Palavras-chave: seleção automática, inversão, reconstrução espectral.

Corresponding author: Nelson Ricardo Coelho Flores Zuniga

[1]Universidade de São Paulo, Instituto de Astronomia, Geofísica e Ciências Atmosféricas (IAG-USP), Departamento de Geofísica. Rua do Matão 1226 - Cidade Universitária 05508-090, São Paulo, SP, Brazil. Phone: +55 11 3091-4755 – E-mail: nelson.zuniga@iag.usp.br
[2]Escola Politécnica da Universidade de São Paulo (POLI-USP), Departamento de Engenharia de Minas e Petróleo. Avenida Professor Luciano Gualberto 380, Cidade Universitária 05508-010, São Paulo, SP, Brazil. Phone: +55 11 3091-5435
[3]Universidade Estadual do Norte Fluminense (UENF), Laboratório de Engenharia e Exploração de Petróleo (LENEP), Avenida Brennand s/n – Imboacica 27910-970, Macaé, RJ, Brazil. Phone: +55 22 2765-6565 – E-mail: slava@lenep.uenf.br

INTRODUCTION

Performing the velocity analysis using an inversion procedure requires the obtaining of the travel-time curve of the target event. This procedure of velocity analysis demonstrated to be very efficient in different applications, such as for converted wave events in near-surface structures (e.g., Bokhonok, 2011; Lu et al., 2018); q-P reflection events in VTI media (e.g., Aleixo and Schleicher, 2010; Golikov and Stovas, 2012); converted waves in VTI media (e.g., Hao and Stovas, 2015; Tseng et al., 2016); OBN data (e.g., Wang and Pham, 2001; Wang et al., 2014); converted waves and OBN data (e.g., Zuniga, 2017; Zuniga et al., 2017 and 2019c); orthorhombic media (e.g., Xu and Stovas, 2018 and 2019); and anisotropic media (e.g., Li and Yuan, 2001; Li, 2003; Farra and Pšenčík, 2018; Abedi and Stovas, 2019a, 2019b). Recently, it was also applied, in different processing conditions, such as using different global search and local search optimization algorithms (e.g., Rios and Sahinidis, 2013; Zuniga, 2017), using topological analysis of objective function (e.g., Larsen, 1999; Li and Yuan, 2003; Bokhonok, 2011; Du and Yan, 2013; Lu et al., 2015; Aleardi et al., 2017; Zuniga et al., 2017, 2018, 2019a) and using L1-norm with derivative-free optimization algorithms (e.g., Ji, 2006; Zhang et al., 2014; Zuniga et al., 2019a, 2019b; Costa et al., 2020).

To extract the travel-times from a reflection event, a not-automated picking is demanded, which increases the processing time and the possibility of performing an ill-picked travel-time curve. So, aiming to minimize the processing time and the error, it is necessary to perform an automated travel-time curve picking to apply an inversion procedure for the velocity analysis step.

Important information of a wavelet (*i.e.*, peak frequency, amplitude and phase) is obtained from frequency-domain when the analysis by decomposing of the spectrum is performed, which allows a better geological characterization. Knowing the sets of peak frequencies and amplitudes which compose a spectrum allows performing better modeling for near-surface analysis (Castagna et al., 2003; Li et al., 2011).

The spectral decomposition technique has been applied for stratigraphic characterization in seismic processing for many different cases, such as time-frequency analysis; short-time Fourier transform; and time-domain spectral decomposition (Chakraborty and Okaya, 1995; Partyka et al., 1999; Liu, 2006; Chen et al., 2008; Liu et al., 2011).

Tomasso et al. (2010) proposed, instead of decomposing the frequencies of a spectrum by time-domain analysis, an approach capable of recomposing single frequencies into a multi-frequency spectrum model. They described the seismic spectrum as a sum of different Ricker wavelet (Ricker, 1953) components. This approach is known as spectral recomposition. However, it is necessary to perform the picking of each pair of amplitude and peak frequency manually. To overcome this limitation, Cai et al. (2013) proposed an estimation of the linear and the nonlinear part of the Ricker wavelet spectrum automatically, based on separating the nonlinear part by least-squares estimation. Thus, the estimation could be automatic for both parts of the spectrum (Golub and Pereyra, 1973). Since the separation of the linear and nonlinear parts of the spectrum is performed, the estimation of the amplitudes and peak frequencies of multiple Ricker components can be then obtained accurately.

In previous works, the spectral recomposition proved to be a very effective manner to obtain wave parameter information (*e.g.* Cai et al., 2013; Zuniga, 2016 and 2017). Then, it can be used to detect a specific wavelet by finding its wave parameters. For a near-surface seismic data processing, it can be very complicated, once the phase varies strongly in short offsets, which is a problem to differentiate reflection events close to each other.

The seismic signal phase, usually, tends to be close to zero and changes this characteristic when it goes through a phase shift resulted from a critical reflection, which changes drastically the Ricker wavelet shape (Hosken, 1988; Wang, 2015). However, for offshore ultra-deep acquisition, the critical point is not usually reached, and the phase

does not use to change significantly, which maintains a shape close to the Ricker wavelet. In this work, we use a zero-phase Ricker wavelet, which already presents subtle distortions due to the interaction with the medium.

Even though, seismic reflection events interfere with each other for being close in time axis, there are structures in which the layers are significantly thick and present strongly different physical properties. These differences present in the seismogram reflection events considerably distant from each other in time axis, in comparison to the reflections above these reflections. So, for a structure like pre-salt from Santos Basin, Brazil, in which there is a very thick salt structure above the carbonate reservoir, there is a significant depth separation, and, therefore, a significant time separation, and, in addition, both geologies present very discrepant physical properties; for this reason, the approach we propose is an effective manner to perform an automated travel-time curve picking for the target interface, since it presents less interference from other reflection events.

Differently from previous applications, the spectral recomposition, in this work, aims to reconstruct the seismic wavelets, related to the target reflection event, of each trace. So, it is necessary to extract the travel-time curve from the target reflection events – the *PP* and *PS* events related to the reflection from the interface between the bottom of the salt layer and the top of the reservoir.

The technique we propose in this work aims to perform an automated travel-time picking from the seismogram trace by trace in a data driven manner, without the need of performing any prior conventional seismic processing step. This technique also allows automated picking even when there is strong random noise. This is possible, once the proposed technique is based on performing the inversion to recover peak frequency and amplitude information of the frequency spectrum of each trace, by calculating the difference between the calculated and the observed spectrum of each wavelet in each trace. The selection of the wavelet related to the target reflection event is performed by comparing and cross-correlating the information recovered in each wavelet of a trace. Thus, the wavelet spectra are compared and separated to determine which of them is the one related to the signal of the target reflection, and which of them is random noise. Then, the workflow is applied to each subsequent trace.

THEORY AND ALGORITHM
Spectral Recomposition

A description of the seismic spectrum as a sum of different Ricker components (Ricker,1953) was proposed by Tomasso et al. (2010), which can be written as

$$d(f) \approx \sum_{i=1}^{n} a_i \psi_i (m_1, f),\qquad(1)$$

where $d(f)$ is the spectrum of a seismic trace; f is the frequency; and a_i and m_i are, respectively, the amplitude and the peak frequency of the i-th Ricker spectrum component, given by

$$R(f) = a\psi(m, f) = a\frac{f^2}{m^2} exp\left(-\frac{f^2}{m^2}\right).\qquad(2)$$

Once the mathematical description of the wavelet is known, it is possible to perform an inversion to fit the calculated frequency spectrum to the observed one of all wavelets in a seismic trace.

The frequency spectrum is found after the application of the Fourier transform in the wavelet. So, each wavelet found in a trace must be transformed into its frequency spectrum before passing through the inversion procedure.

Optimization Criterion

To avoid the use of a global search optimization algorithm, it is proposed to use a multi-start procedure with a local search optimization algorithm (Zuniga, 2017). Nelder-Mead (Nelder and Mead, 1965) optimization algorithm was chosen to be used in this work to optimize the curve fitting between the calculated spectrum to the observed one. The least squares minimization criterion is used to quantify the residual error

between calculated and observed curves. With this, the selection of the number of interactions can be set to adapt the complexity of the spectra of a trace; and with the multi-start procedure, it can be performed by randomizing each initial point for each inversion, which allows obtaining the parameters related to the global minimum region. The statistical distribution can also provide a better understanding of the complexity of the topology of the objective function, which allows determining which kind of optimization algorithm should be used to perform the inversion procedure.

Proposed Algorithm and Technique

We propose a technique and an algorithm based on the reconstruction of the spectrum of a seismic wavelet by performing an inversion procedure in which the spectrum is calculated with a previously proposed mathematical description to fit an observed spectrum. The optimization criterium is also previously proposed in previous section as the mathematical description. Spectral recomposition is performed aiming to recover the signal parameters; however, in the technique we propose, it is possible to observe the variation of peak frequency, amplitude and phase in each wavelet of each trace and not only recovering them. Our technique allows comparing the wavelets among each other in order to separate random noise wavelets from the target signal wavelets (*i.e.*, target reflection event). The algorithm we propose makes it possible by computing the similarities and differences concerning phase, amplitude, frequency and arrival time of the wavelets, which allows finding the wavelet of the target reflection in each trace and its position in the time axis. With this information, it is possible to automatically pick the position of the wavelet in each trace, and then, compose the travel-time curve of the related reflection event.

As the initial step of our proposed algorithm, the curve is calculated to all spectra of the frequencies found in the first trace. Thus, with the information of each pair of frequency and amplitude, there is a comparison of each spectrum with the frequency and amplitude used by the seismic source. The geometrical spreading and attenuation are considered. Additionally, there is a comparison of all the inverted spectra among each other.

The comparison is performed automatically by cross-correlating each peak frequency and amplitude of each spectrum of the trace. The absolute values of peak frequency and amplitude of the spectra are compared among each other. Thus, it is possible to find which of those spectra is related to the signal of the target reflection event, and which of them are related to random noise. This is possible because the most idiosyncratic spectrum in the set is the one associated with the reflection event, and the others similar to each other are related to random noise spectra. This is the main reason to expect complications to perform this automated picking technique for reflections which are too close to each other.

Having defined the wavelet, of the first trace, related to the target reflection event, the technique is applied to the following traces. However, unlike the first trace, we found it is necessary to consider three constraints to perform a more accurate travel-time curve picking:

1. Considering the arrival time of a trace always higher than the previous one, since the next arrival time must take more time to arrive in comparison to the previous one;

2. Comparing the difference between the arrival time of the analysed trace and the arrival time of the previous trace. It restricts the time of the target wavelet between the two arrival times around it since it cannot be lower than the previous arrival time and higher than the next one. The difference of limits can be set according to the different kinds of models, which can present a lithology and/or structure that can generate a more horizontalized reflection event, and, therefore, a narrower time window between the two traces;

3. Comparing and cross-correlating the peak frequency, amplitude, and phase of the spectrum of the signal of the trace, which is being analysed, with the previous one. This third constraint aims to compare the spectrum of the signal of the event in a

trace with the previous one, once they must be very similar to each other and very different from the random noise spectra.

The three constraints must be set according to different characteristics of the medium, seismic source, and kind of reflection event (*PP*, *ShSh*, *SvSv*, *SP* or *PS*), due to the fact that these characteristics may present different sets of arrival times and wavelets. For this reason, it is possible to restrict specific areas of the seismogram, aiming to find the target reflection more quickly.

Muting some parts of the seismogram in which the event is not expected to appear is an interesting manner to minimize the number of wavelets to be inverted, and, therefore, minimize the processing time and enhancing the accuracy. This condition drastically decreases the possibilities of picking the wrong spectrum. However, the muting must be applied only in regions of the seismogram in which there is no relation with the target reflection event, once it can mute important information about the target event when ill-applied.

Once the steps of the technique are applied for each trace and each frequency spectrum related to the signal of the target reflection is obtained, it is possible, after performing the inverse Fourier transform for each trace, to find the arrival time of each wavelet of the event. With the arrival time, for the target reflection event, of each wavelet in its respective trace, the travel-time curve of this reflection event can be drawn.

The described procedure was applied for each PP and PS reflection event of the interface between the bottom of the salt layer and the top of the reservoir for each one of the three models tested in this work. The flowchart of the algorithm is presented in Figure 1.

RESULTS AND DISCUSSION

The three models used in this work are generated by using a finite-difference modelling scheme (Thorbecke and Draganov, 2011), and their parameters are based on three different well log data, from pre-salt from Santos Basin, used by Zuniga (2017). For this reason, we also know the position of each layer and the position in time of each event related to each layer, which allows us to check if the event which was picked with our technique is correct.

The first model tested in this work (Table 1) is composed of a salt structure, in which the 3rd, 4th and 5th layers are part of it, and a carbonate reservoir (V_P = 4010 m/s and V_S = 2012 m/s), which is beneath that structure. The target interface is below the 5th layer, between the bottom of the salt structure and the top of the carbonate reservoir.

In Model 1, the application of the proposed approach was performed for a seismogram without random noise and for the same seismogram with random noise with a signal-noise ratio (*SNR*) of 90% (Fig. 2). Figure 2 shows the output image after our algorithm works; however, in order to present a more friendly visualization, we can observe, in Figure 3, the seismogram using pulses of each arrival for the same seismogram of Figure 2 without noise, and, in Figure 4, the same seismogram of Figure 2 with an *SRN* of 90%. In a closer observation, we can realize, in Figure 5, how difficult it is to perform a conventional picking technique or manual picking. This happens because the target events present low amplitudes for short offsets in comparison to other events, as it can be observed in Figure 5. In Figure 6, we can observe, even more closely, how difficult it is to pick first arrivals of target events. For this reason, our automated picking technique, capable of finding the first arrivals based on reconstructing the spectrum of the wavelets, is strongly desirable for this kind of scenario.

In Figures 2 to 6, it can be observed that the reflections of the *PP* events above the *PP* event related to the target interface (between the bottom of the salt structure and the top of the reservoir) and the *PSv* events above the *PSv* event related to the same target interface are not marked. This happened due to fact that the proposed approach could not find the wavelets related to the target event in the first traces, which, in this approach, forbids the inversion for the subsequent traces. This problem was already expected, since the other reflection events are too similar among them and too close to each other. So, the initial proposition of applying the proposed approach
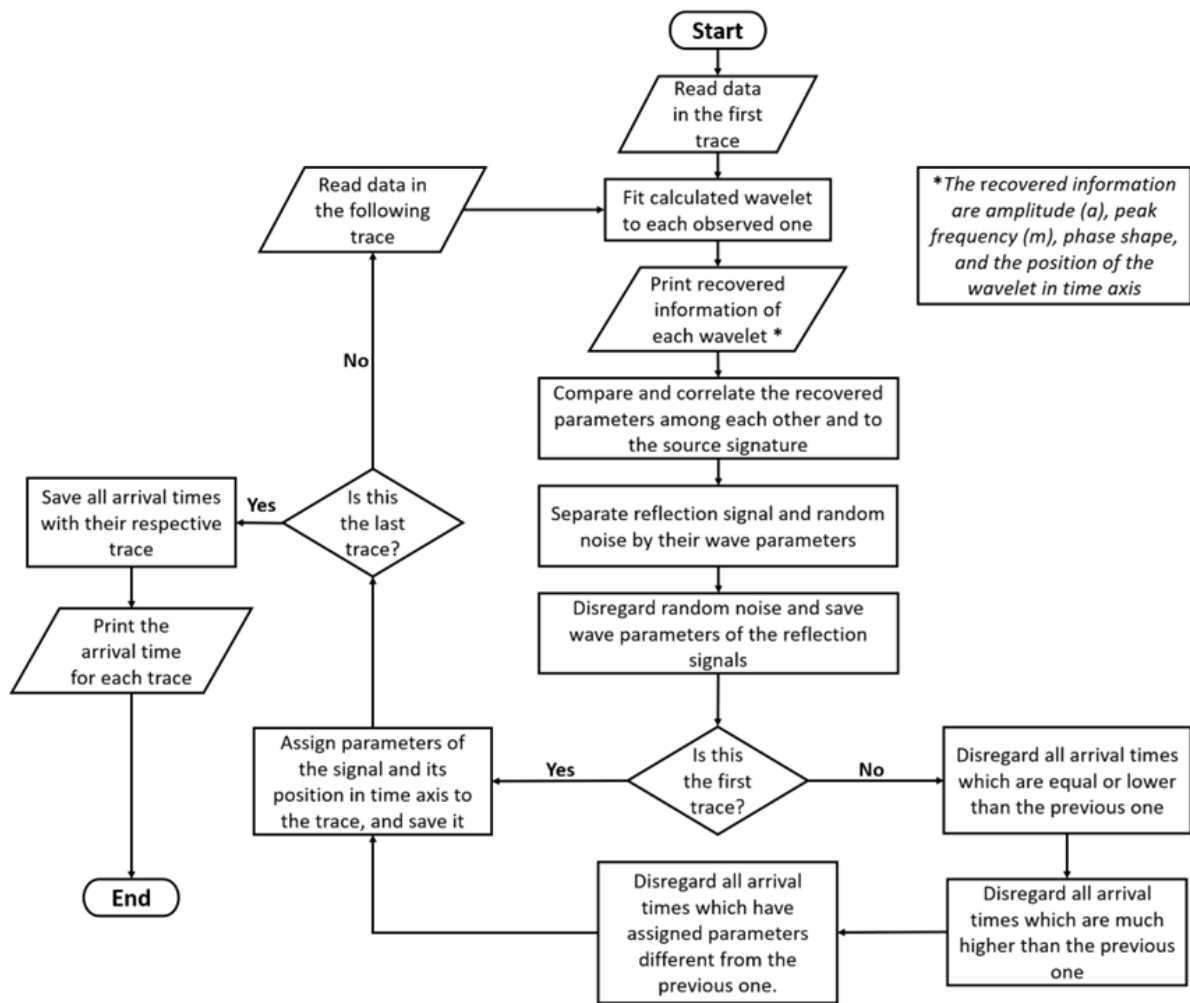
Figure 1 - Flowchart of the implemented algorithm based on our proposed approach.

Table 1 - The parameters of Model 1: Layer thickness (Δz), P-wave velocity (V_P), S-wave velocity (V_S) and V_P/V_S ratio.

Layer	Δz (m)	V_P (m/s)	V_S (m/s)	V_P/V_S
Water	2157	1500	0	-
1	496	2875	1200	2.40
2	108	3505	1628	2.15
3	664	4030	2190	1.84
4	262	5005	2662	1.88
5	1485	4220	2210	1.91

only for the target event succeeded. The red lines, in Figure 2, represent the *PP* and *PSv* reflection events related to the interface between the bottom of the salt and the top of the reservoir. The information concerning the wave parameters of these events was well recovered and the approach provided the possibility of determining all the wavelets related to these target events.

The *PP* event of Model 1, in comparison to the *PSv* event, took less processing time to be found (87% of the processing time for *PSv*), since the *PP* reflection presents a higher amplitude and higher frequency, which allows a better recovering of the information (Cai et al., 2013). The difference in the processing time took to find the target events in the seismogram without random noise was around 4% of the processing time with random noise. However, the accuracy in finding the event was, virtually, the same.

When a window was set, between 2.5 seconds and 7 seconds, aiming to ignore, by muting, the wavelets above and below this range, the processing time decreased to 23% of the total processing time with noise; which is higher than the 4% with no noise, but significantly lower when compared to the complete seismogram with random noise in it.
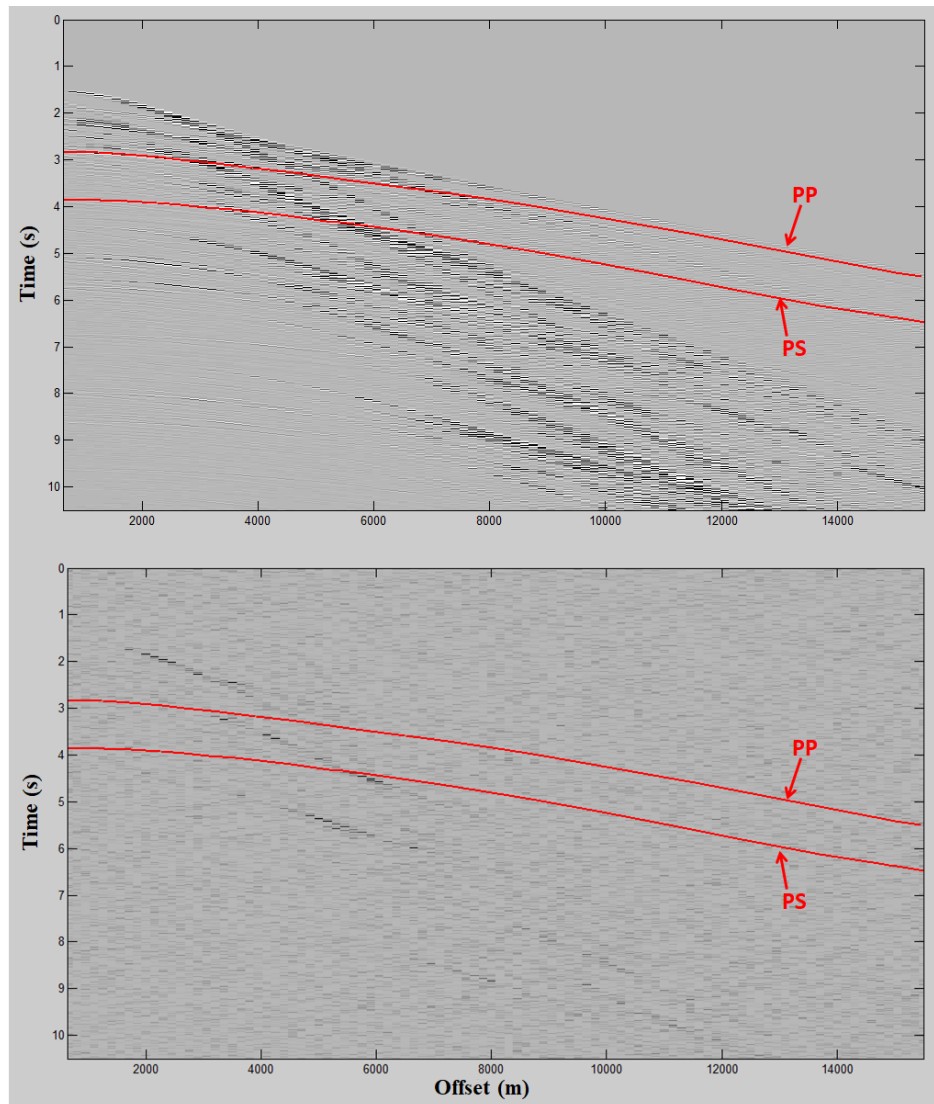
Figure 2 - Seismograms, (above) with no noise and (beneath) with a *SNR* of 90%, of Model 1. The red lines represent the automated picked *PP* and *PSv* events.
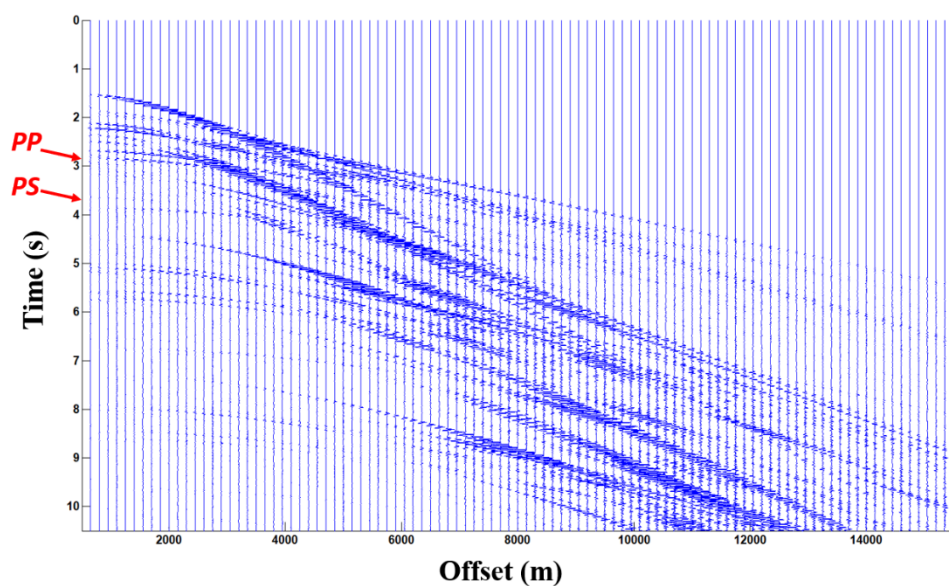

Figure 3 - Seismogram without noise of Model 1 showing wavelets of each arrival. The red arrows indicate the time of first arrivals picked for *PP* and *PSv* events.
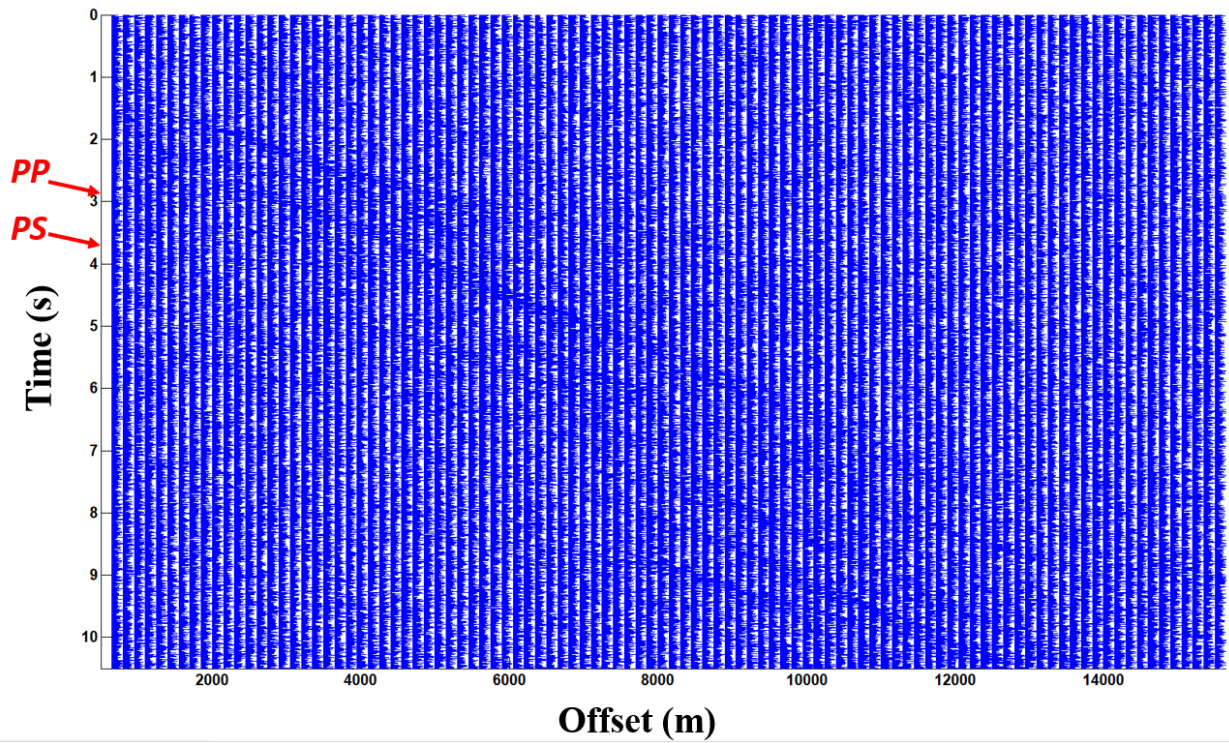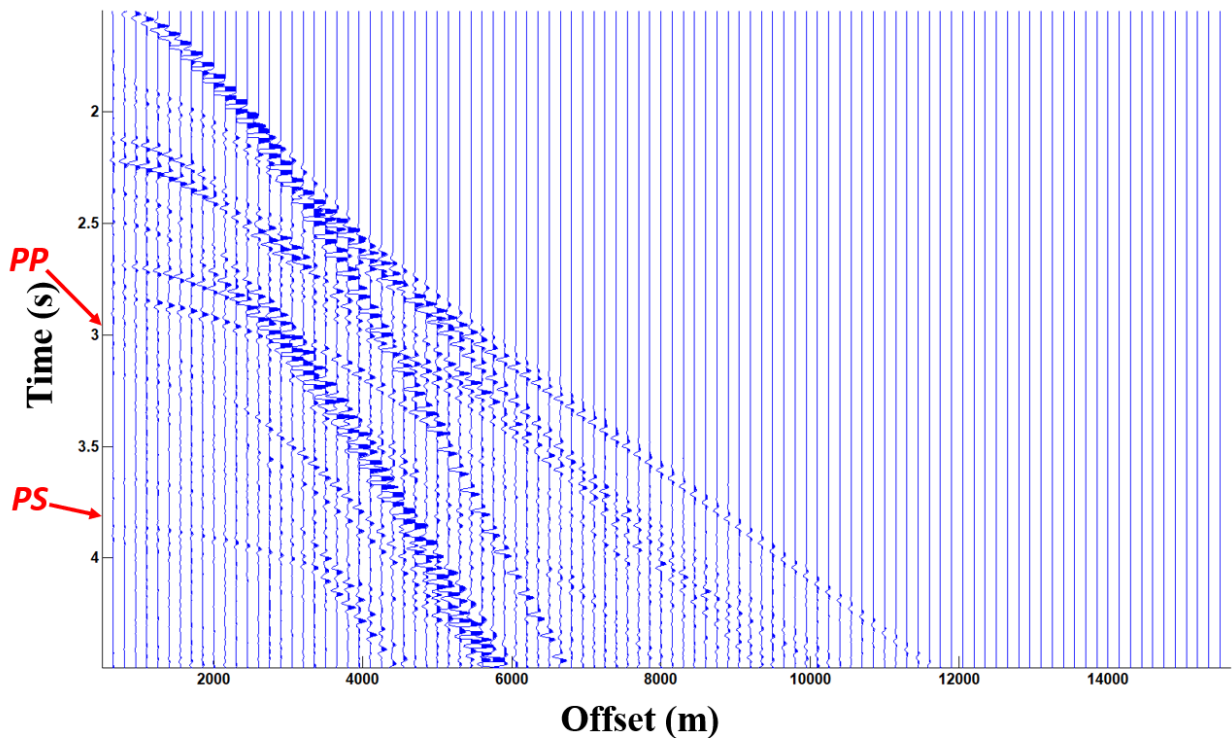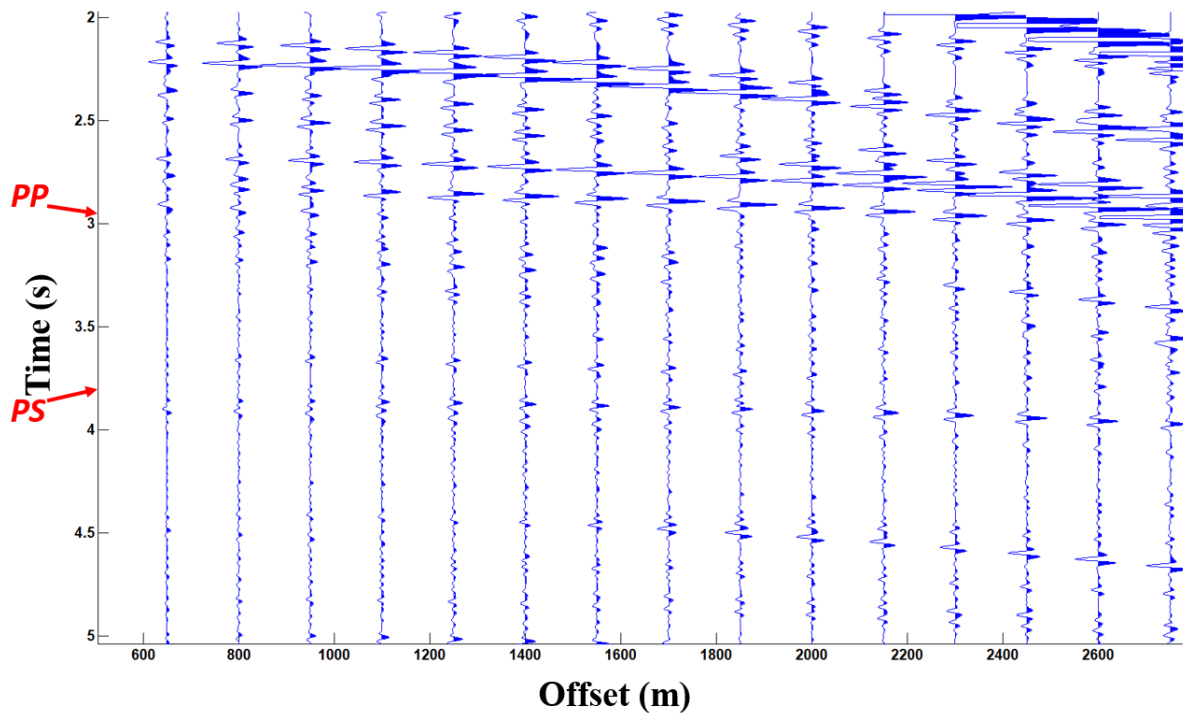
Figure 4 - Seismograms, (above) with no noise and (beneath) with a *SNR* of 90%, of Model 1. The red lines represent the automated picked *PP* and *PSv* events.

Figure 5 - Seismogram without noise of Model 1 showing wavelets of each arrival. The red arrows indicate the time of first arrivals picked for *PP* and *PSv* events.

Figure 6 - Crop between 500 and 2800 m of the seismogram in Figure 5. The red arrows indicate the time of first arrivals picked for *PP* and *PSv* events.

In Model 2 (Table 2), a carbonate reservoir (V_P = 3599 m/s and V_S = 1800 m/s), under the 4th, 5th and 6th layers of a salt structure, is presented. For this model, the same conditions (as for Model 1) were applied regarding the noise, in which the seismogram with no noise and with *SNR* of 90% is shown. The target interface is below the 6th layer, between the bottom of the salt structure and the top of the carbonate reservoir.

Table 2 - The parameters of Model 2: Layer thickness (Δz), *P*-wave velocity (V_P), *S*-wave velocity (V_S) and V_P/V_S ratio.

Layer	Δz (m)	V_P (m/s)	V_S (m/s)	V_P/V_S
Water	2101	1500	0	-
1	431	2852	1190	2.40
2	82	3390	1512	2.24
3	525	3461	1590	2.18
4	212	3801	1885	2.02
5	1151	4321	2219	1.95
6	503	3820	1899	2.01

In Model 2 (Fig. 7 to 11), it is possible to observe that the same limitations were found in determining the other events that were not the target events, similarly to Model 1; however, the same information was obtained in Model 2, which corroborates the effectiveness of the proposed approach in recovering the wave parameter information to find the target events.

Model 2 presents more layers than Model 1, which increased the processing time - however, did not change the accuracy - since the processing time for this model was 79% of the total processing time presented in Model 1.

The processing time found in Model 2, to find the PP reflection event, was around 84% of the processing time to find the PSv event; and the average processing time, to find the target events in the seismogram with no noise, was around of 5% of the processing time to find these events in the seismogram with random noise.

Setting the same time window as before (between 2.5 seconds and 7 seconds), an average processing time around 29% of the time used to find the target events with *SNR* of 90% was found.
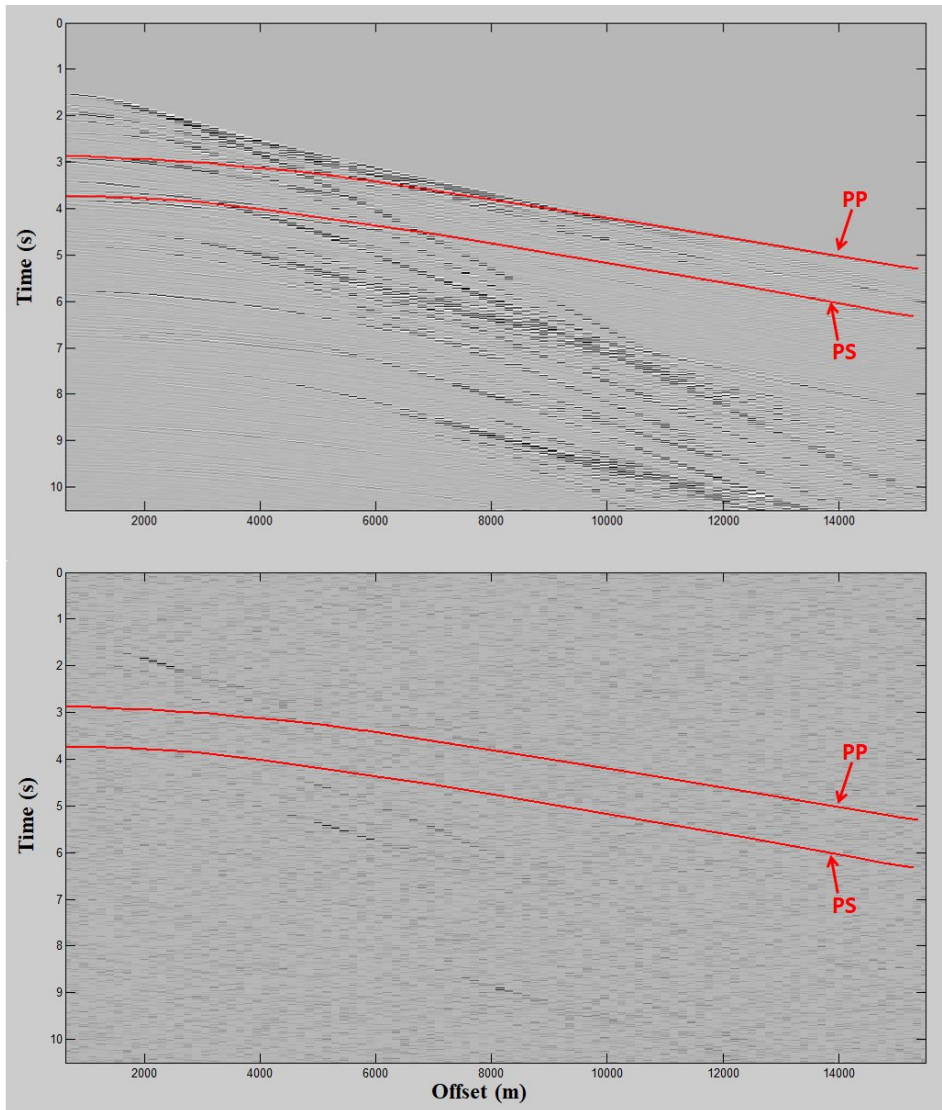
Figure 7 - Seismograms, (above) with no noise and (beneath) with a *SNR* of 90%, of Model 2. The red lines represent the automated picked *PP* and *PSv* events.
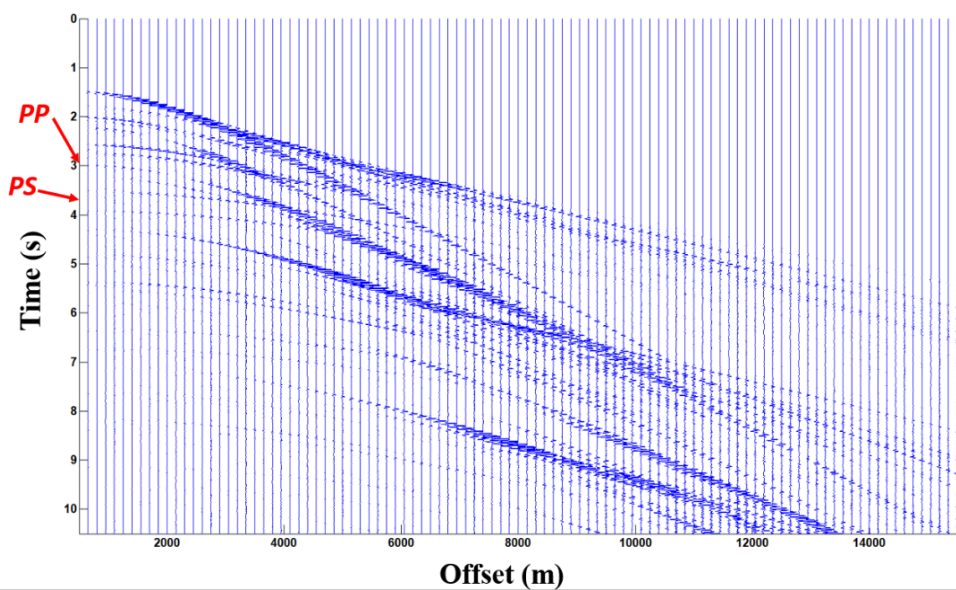

Figure 8 - Seismogram without noise of Model 2 showing wavelets of each arrival. The red arrows indicate the time of first arrivals picked for *PP* and *PSv* events.
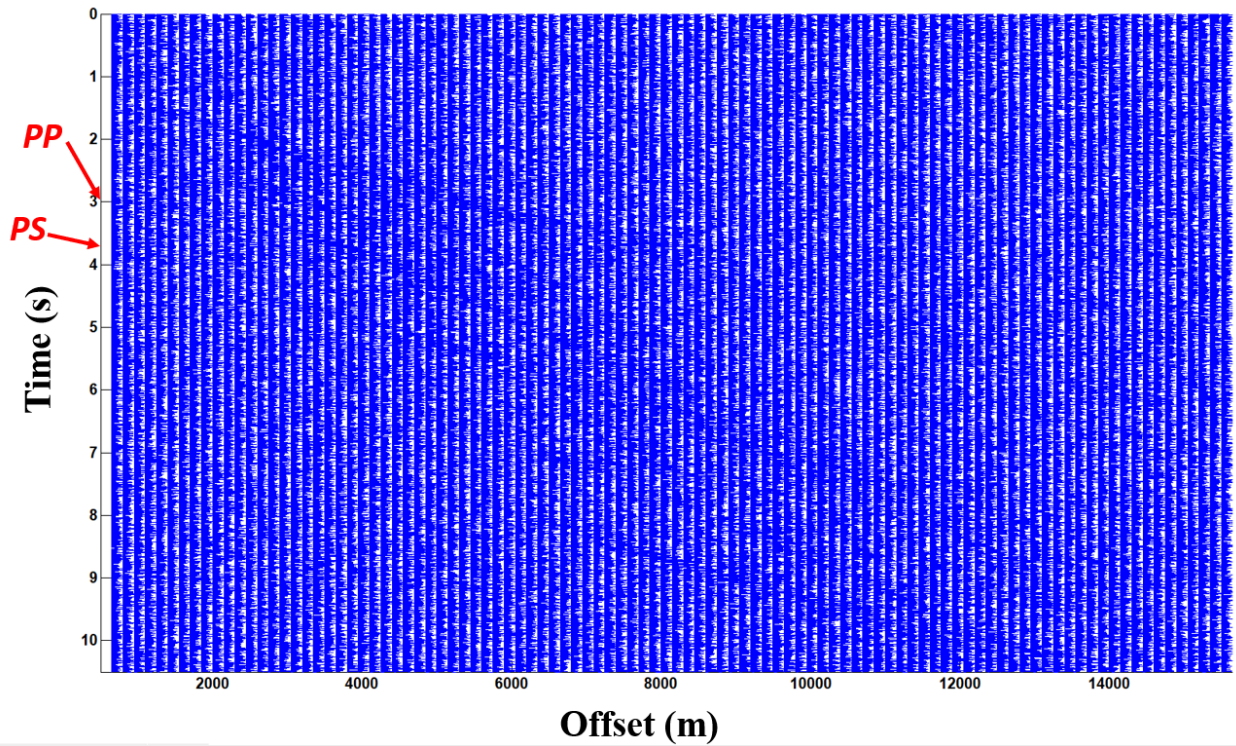
Figure 9 - Seismogram with a *SNR* of 90% of Model 2 showing wavelets of each arrival. The red arrows indicate the time of first arrivals picked for *PP* and *PSv* events.
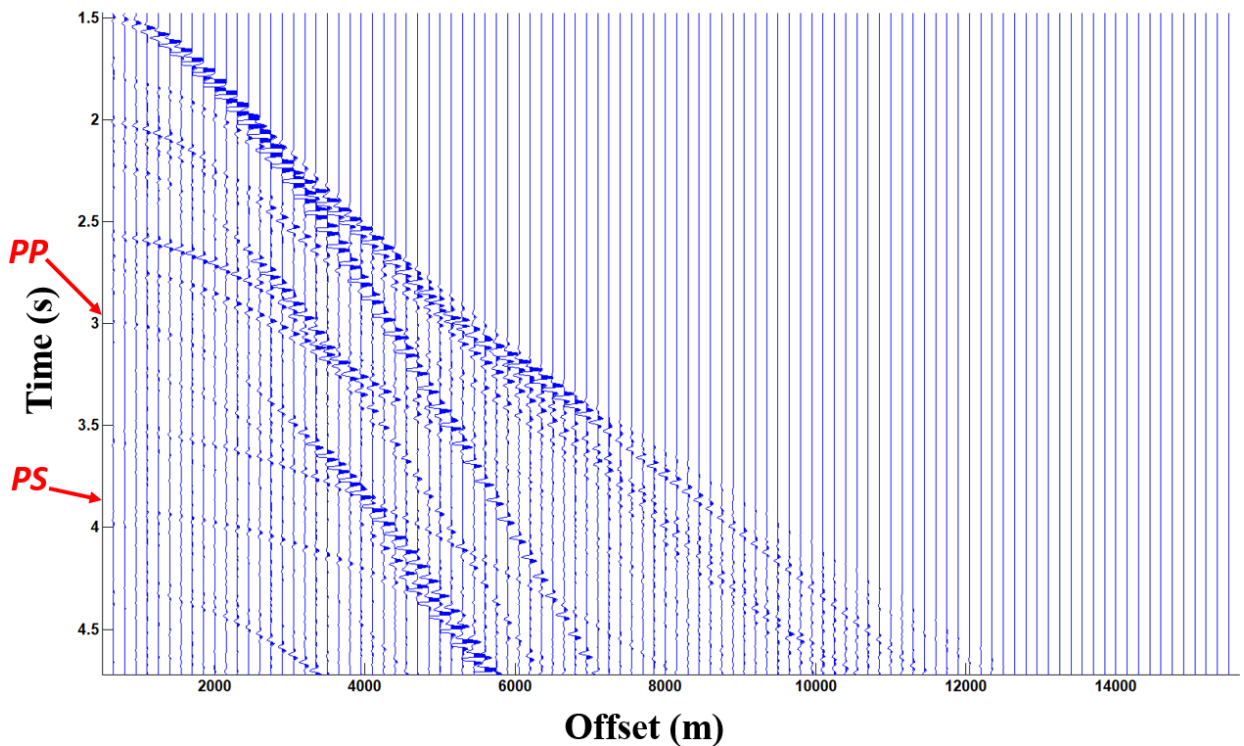

Figure 10 - Crop between 1.47 and 4.70 seconds of the seismogram in Figure 8. The red arrows indicate the time of first arrivals picked for *PP* and *PSv* events.
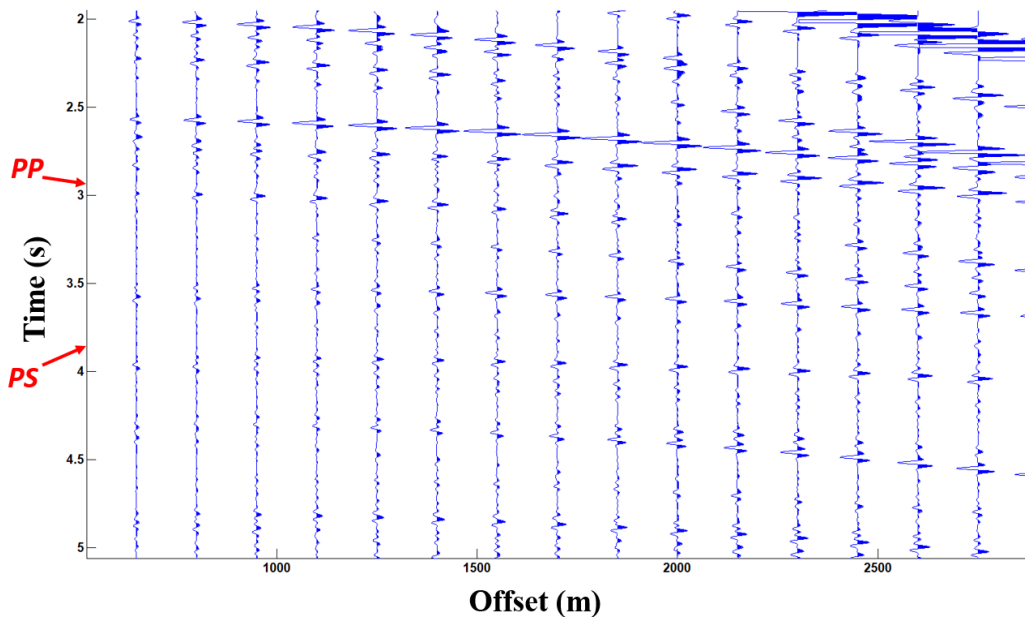
Figure 11 - Crop between 500 and 2900 m of the seismogram in Figure 10. The red arrows indicate the time of first arrivals picked for *PP* and *PSv* events.

Differently from the previous two models tested in this work, Model 3 presents a velocity abnormally low in the salt structure (Table 3). The 6th layer presents a velocity significantly lower than the underlying layer (7th layer), which is not uncommon; however, the 6th layer also presents a lower velocity than the 5th layer, the one above it. This kind of velocity variation in a salt structure (composed by the 5th, 6th and 7th layers) is not commonly found above a carbonate reservoir, which in this case presents V_P = 3814 m/s and V_S = 1995 m/s. The target interface is below the 7th layer, between the bottom of the salt structure and the top of the carbonate reservoir.

Table 3 - The parameters of Model 3: Layer thickness (Δz), *P*-wave velocity (V_P), *S*-wave velocity (V_S) and V_P/V_S ratio.

Layer	Δz (m)	V_P (m/s)	V_S (m/s)	V_P/V_S
Water	2159	1500	0	-
1	342	2879	1220	2.36
2	167	3411	1599	2.13
3	294	3502	1650	2.12
4	628	3680	1665	2.21
5	1071	4535	2190	2.07
6	154	3912	1899	2.06
7	134	4550	2210	2.06

More complex models certainly present a more challenging condition to use the approach proposed in this work. Therefore, it was already expected to have higher processing times to find the target events in this model, in which more layers than the two previous models are found. Initially, in the seismogram (Fig. 12 to 16) without noise, a processing time of 7%, in comparison to the total processing time of the seismogram with noise, was found. It shows that the processing time increased significantly, in comparison to the other two models. The processing time to find the PP event, in comparison to the PSv event, is around 85%, which shows that the increased complexity of the model does not result in increasing the complexity of finding the converted wave event in comparison to the conventional event.

Setting the same time window set for the previous two models (between 2.5 seconds and 7 seconds), to find the target events, resulted in an average processing time around 56% of the time to find the events in the whole seismogram.

The average processing time to find the target events, in this model, was significantly higher in comparison to the other two models - Model 1 showed 71% and Model 2 showed 75% of the average processing time in Model 3.
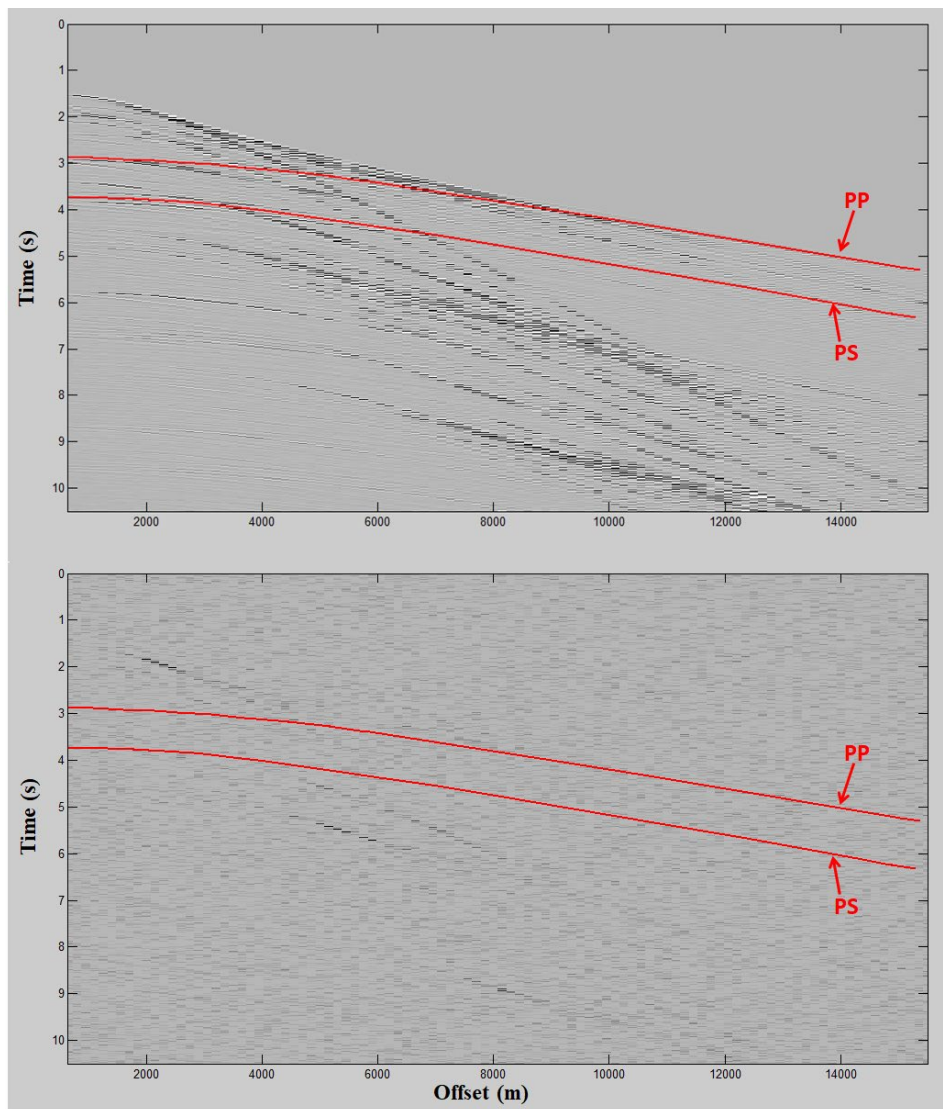
Figure 12 - Seismograms, (above) with no noise and (beneath) with a *SNR* of 90%, of Model 3. The red lines represent the automated picked *PP* and *PSv* events.
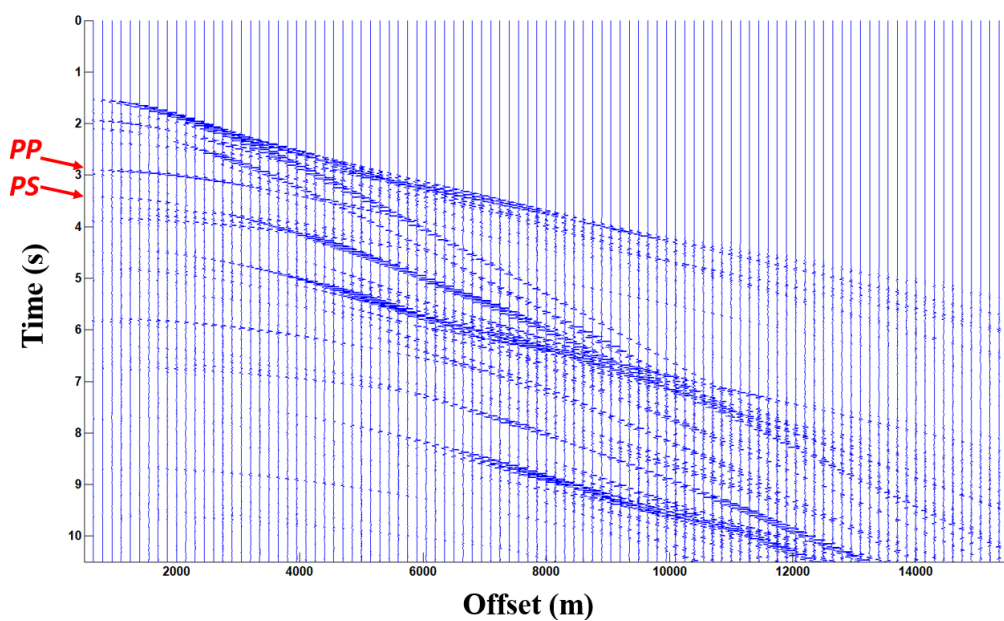

Figure 13 - Seismogram without noise of Model 3 showing wavelets of each arrival. The red arrows indicate the time of first arrivals picked for *PP* and *PSv* events.
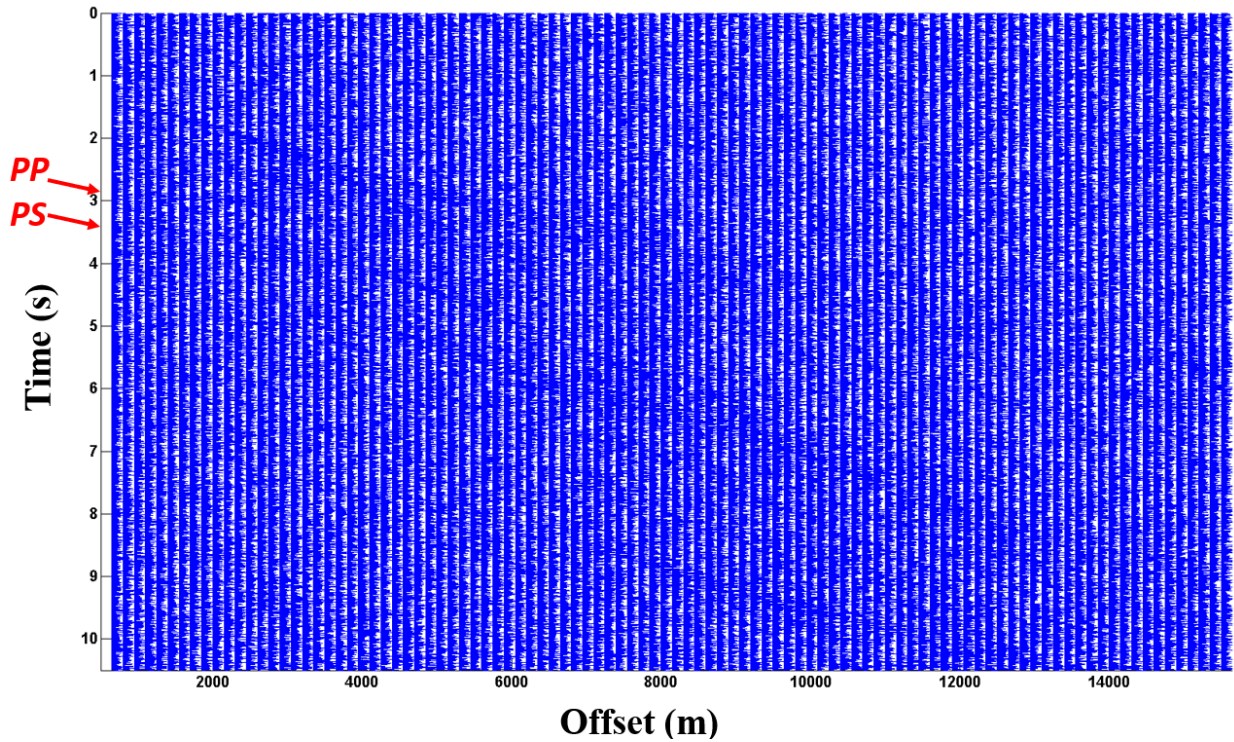
Figure 14 - Seismogram with a *SNR* of 90% of Model 3 showing wavelets of each arrival. The red arrows indicate the time of first arrivals picked for *PP* and *PSv* events.
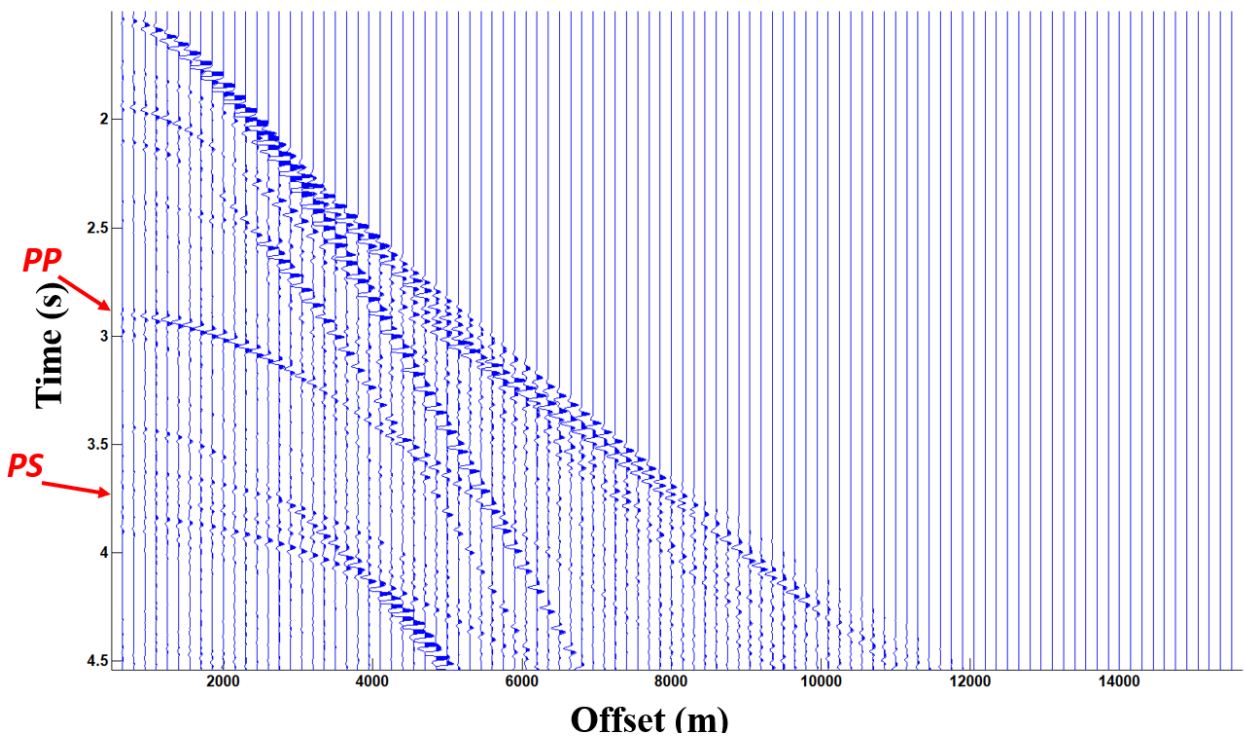

Figure 15 - Crop between 1.5 and 4.5 seconds of the seismogram in Figure 13. The red arrows indicate the time of first arrivals picked for *PP* and *PSv* events.
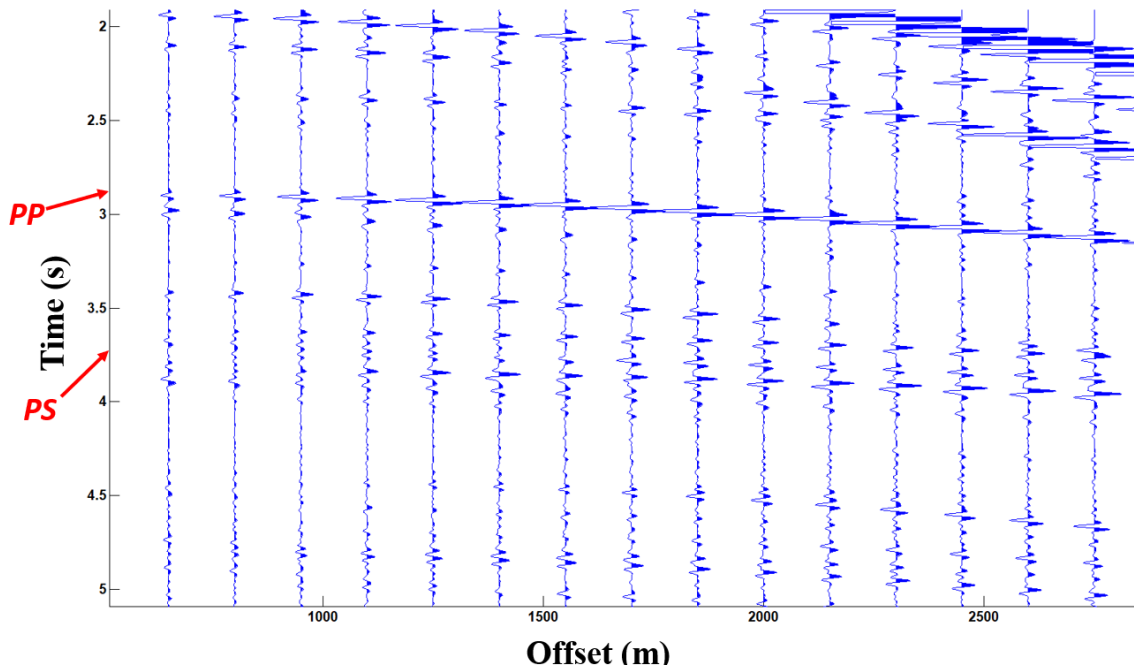
Figure 16 - Crop between 500 and 2700 m of the seismogram in Figure 15. The red arrows indicate the time of first arrivals picked for *PP* and *PSv* events.

CONCLUSIONS

The technique we propose in this work presented to be a very efficient manner to obtain the travel-time curve of the target event by finding the wavelets in each trace which, together, compose the reflection event. Our approach aims to perform this in a data driven manner, without the need of performing any prior conventional seismic processing step. This technique found the *PP* and *PSv* reflection events very accurately, which allows extracting their travel-time curves. With these travel-times, essential information to perform the velocity analysis step with an inversion procedure, the obtaining of velocity information can be performed much more accurately and quickly.

The complexity of the model and the kind of reflection event (*PP* or *PS*) are factors which influence the processing time, increasing it when the converted event is the target one, and also when the model presents complex structures and geologies; however, it is not a factor that increases or decreases the accuracy in obtaining the travel-time curve, in a significant manner.

The technique we propose in this work showed to be very effective to extract the travel-time curves of the conventional and converted reflection events related to the interface between the bottom of the salt structure and the top of the reservoir. The effectiveness of our technique could be observed even with strong random noise in the seismogram. The performance of our technique can be significantly increased, concerning the processing time, when parts of the seismogram, related to the reflections of overlying interfaces, are muted. It is important to note that this method was not tested for irregular geometries, and may have some difficulty in being effective for irregular geometries in which there is back scattering. On the other hand, our proposed technique is not recommended to be applied in much shallower reservoirs or to find the reflections related to interfaces close to each other, as it showed to be ineffective to find the reflection events of the shallower interfaces, since the events are located too close to each other.

ACKNOWLEDGEMENTS

REFERENCES

Abedi, M. M., Stovas, A., 2019a. Extended generalized non-hyperbolic moveout approximation. Geophysical Journal International, 216(2): 1428–1440.

Abedi, M. M., Stovas, A., 2019b. A new parameterization for generalized moveout approximation, based on three rays. Geophysical Prospecting, 67(5): 1243–1255.

Aleardi, M., Ciabarri, F., Mazzotti, A., 2017. Probabilistic estimation of reservoir properties by means of wide-angle AVA inversion and a petrophysical reformulation of the Zoeppritz equations. Journal of Applied Geophysics, 147: 28–41.

Aleixo, R., Schleicher, J., 2010. Traveltime approximations for q-P waves in vertical transversely isotropic media. Geophysical Prospecting, 58: 191–201.

Bokhonok, O., 2011. Sísmica de Reflexão Rasa Multicomponente: Aquisição e inversão de tempos de trânsito e amplitudes. PhD Thesis, Universidade de São Paulo, SP, Brazil, 162 pp.

Cai, Y., Fomel, S., Zeng, H., 2013. Automated spectral recomposition with application in stratigraphic interpretation. Interpretation, 1(1): 109–116.

Castagna, J. P., Sun, S., Siegfried, R. W., 2003. Instantaneous spectral analysis: Detection of low-frequency shadows associated with hydrocarbons. The Leading Edge, 22: 120–127.

Chakraborty, A., Okaya, D., 1995. Frequency-time decomposition of seismic data using wavelet-based methods. Geophysics, 60: 1906–1916.

Chen, G., Matteucci, G., Fahmy, B., Finn, C., 2008. Spectral-decomposition response to reservoir fluids from a deepwater West Africa reservoir. Geophysics, 73: C23-C30.

Costa, F. T., Santos, M. A. C., Soares Filho, D. M., 2020. Wavenumbers illuminated by time-domain acoustic FWI using the L1 and L2 norms. Journal of Applied Geophysics, 174: 103935.

Du, Q., Yan, H., 2013. PP and PS joint AVO inversion and fluid prediction. Journal of Applied Geophysics, 90: 110–118.

Farra, V., Pšenčík, I., 2018. Reflection moveout approximation for a P-SV wave in a moderately anisotropic homogeneous VTI layer. Geophysics, 84(2): C75-C83.

Golikov, P., Stovas, A., 2012. Accuracy comparison of nonhyperbolic moveout approximations for qP-waves in VTI media. Journal of Geophysics and Engineering, 9: 428–432.

Golub, G. H., Pereyra, V., 1973. The differentiation of pseudo-inverses and nonlinear least-squares problems whose variables separate. Numerical Analysis, 10: 413–432.

Hao, Q., Stovas, A., 2015. Generalized moveout approximation for P-SV converted waves in vertically inhomogeneous transversely isotropic media with a vertical symmetry axis. Geophysical Prospecting, 64(6): 1469–1482.

Hosken, J. W. J., 1988. Ricker wavelets in their various guises. First Break, 6(1): 24–33.

Ji, J., 2006. Hybrid L1/L2 norm IRLS method with application to velocity-stack inversion. In: 68th EAGE Conference and Exhibition incorporating SPE EUROPEC. Expanded Abstract, Vienna, Austria.

Larsen, J. A., 1999. AVO Inversion by Simultaneous P-P and P-S Inversion. 1999. (Master's Thesis) - University of Calgary, Department of Geology and Geophysics, Calgary. Canada. 124 pp.

Li, X. Y. 2003. Converted-wave moveout analysis revisited: The search for a standard approach. In: 73rd Annual International Meeting, Society of Exploration Geophysics, Expanded Abstract, Dallas, Texas, USA, p. 805-808.

Li, X. Y., Yuan, J., 2001. Converted wave imaging in inhomogeneous, anisotropic media: Part I. Parameter estimation. In: 63rd EAGE Conference. Expanded Abstract, Amsterdam, Netherlands, v. 1, p. 109.

Li, X. Y., Yuan, J., 2003. Converted-wave moveout and conversion-point equations in layered VTI media: theory and applications. Journal of Applied Geophysics, 54(3–4): 297–318.

Li, Y., Zheng, X., Zhang, Y., 2011. High-frequency anomalies in carbonate reservoir characterization using spectral decomposition. Geophysics, 76: V47-V57.

Liu, J., 2006. Spectral Decomposition and Its Application in Mapping Stratigraphy and Hydrocarbons. Ph.D. thesis, University of Houston, TX, USA. 115 pp.

Liu, G., Fomel, S., Chen, X., 2011. Time-frequency

analysis of seismic data using local attributes. Geophysics, 76: P23-P34.

Lu, J., Yang, Z., Wang, Y., Shi, Y., 2015. Joint PP and PS AVA seismic inversion using exact Zoeppritz equations. Geophysics, 80(5): R239-R250.

Lu, J., Wang, Y., Chen, J., 2018. Joint velocity updating for anisotropic PP and PS prestack time migration based on hyperbolic correction of nonhyperbolic moveout. Journal of Geophysics and Engineering, 15(4): 1171–1186.

Nelder, J. A., Mead, R., 1965. A simplex method for function minimization. The Computer Journal 7, 308–313.

Partyka, G. J., Gridley, J., Lopez, J., 1999. Interpretational applications of spectral decomposition in reservoir characterization. The Leading Edge, 18: 353–360.

Ricker, N., 1953. The form and laws of propagation of seismic wavelets. Geophysics, 18: 10–40.

Rios, L. M; Sahinidis, N. V., 2013. Derivative-free optimization: A review of algorithms and comparison of softwares implementations. Journal of Global Optimization, 56: 1247–1293.

Thorbecke, J. W., Draganov, D., 2011. Finite-difference modeling experiment for seismic interferometry. Geophysics, 76: H1-H18.

Tomasso, M., Bououllec, R., Pyles, D. R., 2010. The use of spectral recomposition in tailored forward seismic modeling of outcrop analogs. AAPG Bulletin, 94: 457–474.

Tseng, P. Y., Chang, Y. F., Chen, C. H., Shih, R. C., 2016. Traveltimes and conversion-point positions for P-SV converted wave propagation in a transversely isotropic medium: Numerical calculations and physical model studies. Exploration Geophysics, 49(1): 30–41.

Wang, Y., 2015. Generalized seismic wavelets. Geophysical Journal International, 203(2): 1172–1178.

Wang, W., Pham, L. D., 2001. Converted-wave prestack imaging and velocity analysis by pseudo-offset migration. In: 63rd EAGE Conference. Expanded Abstract, Amsterdam, Netherlands, L–12.

Wang, P. L., Junfeng, C. Y., Hu, T., 2014. Converted-wave imaging technology and application for complex structures. Exploration Geophysics, 45(2): 105–115.

Xu, S., Stovas, A., 2018. Estimation of the conversion point position in elastic orthorhombic media. Geophysics, 84(1): C15-C25.

Xu, S., Stovas, A., 2019. Traveltime approximation for converted waves in elastic orthorhombic media. Geophysics, 84(5): C229-C237.

Zhang, F., Dai, R. Liu, H., 2014. Seismic inversion based on L1-norm misfit function and total variation regularization. Journal of Applied Geophysics, 109: 111–118.

Zuniga, N. R. C. F., 2016. Inversion of wave parameters to perform spectral recomposition, Brazil. In: VII Simpósio Brasileiro de Geofísica - SimBGf. Ouro Preto, MG, Brazil. SBGf.

Zuniga, N. R. C. F., 2017. Inversion of wave parameters to perform spectral recomposition of GPR data. In: 15th SBGf International Congress. Rio de Janeiro, RJ, Brazil, 129–132.

Zuniga, N. R. C. F., Molina, E. C., Prado, R. L., 2017. Comparison of travel-time approximations for unconventional reservoirs from Santos Basin, Brazil. Brazilian Journal of Geophysics, 35(4): 271–286.

Zuniga, N. R. C. F., Ribeiro, F. B., Priimenko, V. I., 2018. Relation between the model and the topography of the objective function in a velocity analysis using a nonhyperbolic multicomponent travel-time approximation. Revista Brasileira de Geofísica, 36(4): 375–384.

Zuniga, N. R. C. F., Ribeiro, F. B., Priimenko, V. I., 2019a. L2- and L1-norm of nonhyperbolic travel-time. Brazilian Journal of Geophysics, 37(2): 155–161.

Zuniga, N. R. C. F., Ribeiro, F. B., Priimenko, V. I., 2019b. Comparison of L2- and L1-norm to perform the inversion of travel-time curves using nonhyperbolic multiparametric approximations with unimodal and multimodal behavior. Brazilian Journal of Geophysics, 37(3): 291–297.

Zuniga, N. R. C. F., Molina, E. C., Prado, R. L., 2019c. Comparative analysis of nonhyperbolic travel-time approximations of multicomponent seismic data using OBN technology. Brazilian Journal of Geophysics, 37(4): 397–407.

N.R.C.F.Z.: Developed the proposed approach and implemented the algorithm used in this paper; **V.I.P.:** Developed the proposed approach.